Supporting information

Phosphorescent 2-, 3-, and 4-coordinate cyclic alkyl amino carbene (CAAC) Cu(I) complexes

Rasha Hamze,[a] Rodolphe Jazzar,[b] Michele Soleilhavoup,[b] Peter I. Djurovich,[a] Guy Bertrand[b] and Mark E. Thompson[a]
Department of Chemistry, University of Southern California, Los Angeles, California 90089
Department of Chemistry, University of California, San Diego, La Jolla, California 92023
E-mail: met@usc.edu

General Information

Synthesis. All reactions were performed under nitrogen atmosphere in oven dried glassware. Potassium dihydrotris(1-pyrazolyl)borate K[pz_3BH] (KTp) and Chloro[1,3-bis(2,6-di-i-propylphenyl)imidazol-2-ylidene]copper(I) (IPr)CuCl and were purchased from Sigma-Aldrich. KTp was washed with cold toluene before use to remove traces of excess pyrazole. Tetrahydrofuran and dichloromethane were purified by Glass Contour solvent system by SG Water USA, LLC. (1-(2,6-diisopropylphenyl)-3,3-diethyl-5,5-dimethylpyrrolidin-2-ylidene)copper(I) chloride (**1-Cl**)[3, 4] and ((1R,3S,5r,7r)-1'-(2,6-diisopropylphenyl)-4',4'-dimethylspiro[adamantane-2,3'-pyrrolidin]-2'-ylidene)copper(I) chloride (**2-Cl**)[5] were synthesized according to literature procedures. Dry, air-free methylcyclohexane (MeCy) and 2-methyltetrahydrofuran (2-MeTHF) were purchased from Sigma-Aldrich and used without further purification. ^{1}H and ^{13}C NMR spectra were recorded on a Varian Mercury 400. The chemical shifts are given in units of ppm and referenced to the residual proton resonance of acetone ($(CD_3)_2CO$) at 2.05 ppm. Elemental analyses were performed at the University of Southern California, CA.

DFT Calculations. All calculations were performed using Jaguar[6] 9.1 software package on the Schrodinger Material Science Suite (v2016-4). Gas phase geometry optimization was calculated using B3LYP[7, 8] functional with the LACVP**[9] basis set as implemented in Jaguar. Geometric parameters obtained from XRD analyses were used as a starting point for single point calculations on the ground state and geometry optimization was performed on the triplet state.

Photophysical characterization. The UV-visible spectra were recorded on a Hewlett-Packard 4853 diode array spectrometer. Steady state emission measurements were performed using a QuantaMaster Photon Technology International spectrofluoremeter. All reported spectra are corrected for photomultiplier response. Phosphorescence lifetime measurements were performed using an IBH Fluorocube instrument equipped with 281 nm and 331 nm LED excitation sources using time-correlated single photon counting method. Quantum yields at room temperature were measured using a Hamamatsu C9920 system equipped with a xenon lamp, calibrated integrating sphere and model C10027 photonic multichannel analyzer (PMA). All samples were deaerated by bubbling N_2 in a quartz cuvette fitted with a Teflon stopcock.

XRay Crystallography. The single-crystal X-ray diffraction data for compounds **1** – **3-Tp** were collected on a Bruker SMART APEX DUO three-circle platform diffractometer with the χ axis fixed at 54.745° and using Mo Kα radiation (λ = 0.710 73 Å) monochromated by a TRIUMPH curved-crystal monochromator. The crystals were mounted in Cryo-Loops using Paratone oil. Data were corrected for absorption effects using the multiscan method (SADABS). The structures were solved by direct methods and refined on F2 using the Bruker SHELXTL software package. All non-hydrogen atoms were refined anisotropically.

Synthesis of CAAC^{Et2}-CuTp (1-Tp)

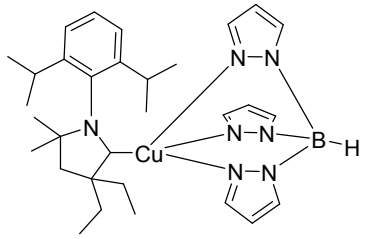

In the glovebox, CAAC^{Et2}-CuCl **1-Cl** (78 mg, 0.196 mmol) and KTp (54 mg, 0.216 mmol) were mixed in THF and stirred at room temperature for 2 hours. The reaction mixture was then filtered under inert atmosphere through a plug of celite, and the solvent was removed under reduced pressure. The obtained yellow powder was dried under vacuum for 3 days (95 mg, 85%). Single crystals were grown by layering dry hexane over a concentrated solution of the complex in THF under inert atmosphere. ^{1}H NMR (400 MHz, Acetone-d_6, δ) 7.51 (t, J = 8.2 Hz, 1H), 7.49 (d, *J* = 2.7 Hz, 3H), 7.39 (d, *J* = 7.9 Hz, 2H), 6.77 (s, 3H), 5.91 (d, *J* = 2.0 Hz, 3H), 3.20 (sept, J = 6.76 Hz, 2H), 2.14 (s, 6H), 1.43 (s, 6H), 1.31 (d, *J* = 6.8 Hz, 6H), 1.19 (t, J = 7.48 Hz, 6H), 0.94 (d, *J* = 6.7 Hz, 6H). ^{13}C NMR (101 MHz, acetone-d$_6$, δ) 147.11, 140.24, 138.26, 133.98, 129.34, 103.62, 80.64, 64.79, 41.08, 32.66, 29.99, 29.95, 27.37, 23.13. Carbene carbon not observed. Elemental Analysis: Anal. Cacld. for $C_{30}H_{43}BCuN_7$ + 0.5 H_2O: C, 62.2; H, 7.74; N, 16.4. Found: C, 62.3; H, 7.46; N, 16.4.

Synthesis of CAAC^{Ad}-CuTp (2-Tp)

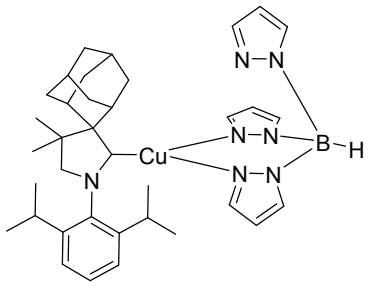

Same method as **1-Tp**. CAAC^{Ad}-CuCl **2-Cl** (100 mg, 0.223 mmol); KTp (62 mg, 0.245 mmol). Yellow powder product (132 mg, 83%). Single crystals grown by same method as **1-Tp**. ^{1}H NMR (400 MHz, Acetone-d$_6$, δ) 7.48 (t, J = 7.7 Hz, 1H), 7.39 (d, J = 2.0 Hz, 3H), 7.33 (d, J = 7.7 Hz, 2H), 6.97 (d, J = 1.4 Hz, 3H), 5.94 (t, J = 2 Hz, 3H), 3.78 (d, J = 13.6 Hz, 3H), 3.09 (sept, J = 6.68 Hz, 2H), 2.40 (s, 2H), 2.23 – 2.09 (m, 5H), 1.95 – 1.73 (m, 8H), 1.65 (d, J = 12.6 Hz, 2H), 1.38 (s, 6H), 1.28 (d, J = 6.7 Hz, 6H), 0.82 (d, J = 6.7 Hz, 5H). ^{13}C NMR (101 MHz, acetone-d$_6$, δ) 146.97, 140.59, 138.02, 134.51, 129.50, 125.64, 103.95, 77.72, 66.35, 48.31, 39.44, 37.98, 36.07, 35.28, 29.88, 29.58, 28.36, 27.00, 23.69. Carbene carbon not observed. Elemental Analysis: Anal. Cacld. for $C_{36}H_{50}BCuN_7$ + 0.5 H_2O: C, 65.2; H, 7.60; N, 14.8. Found: C, 65.0; H, 7.48; N, 14.7.

Synthesis of IPrCuTp (3-Tp)

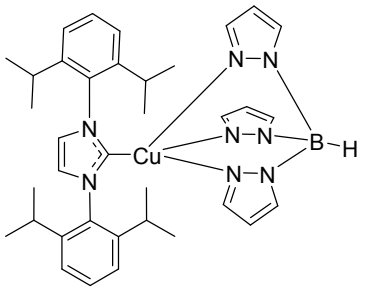

Same method as **1-Tp**. IPrCuCl (150 mg, 0.308 mmol); KTp (85 mg, 0.338 mmol). White powder product (188 mg, 92%). Single crystals grown by same method as **1-Tp**. ^{1}H NMR (400 MHz, Acetone-d_6, δ) 7.53 (s + t, 2H + 2H (J = 7.82 Hz) respectively), 7.37 (d, J = 7.8 Hz, 4H), 7H), 7.34 (d, J = 2 Hz, 3H), 6.27 (d, J = 1.5 Hz, 3H), 5.77 (t, J = 2Hz, 3H), 3.08 (t, J = 6.9 Hz 4H), 1.22 (d, J = 6.9 Hz, 12H), 1.05 (d, J = 6.9 Hz, 12H). ^{13}C NMR (101 MHz, acetone-d_6, δ) 147.21, 140.34, 138.46, 133.77, 130.34, 124.69, 124.14, 29.21, 24.85, 24.14. Carbene carbon not observed. Elemental Analysis: Anal. Cacld. for $C_{36}H_{46}BCuN_8$ + H_2O: C, 63.3; H, 7.08; N, 16.4. Found: C, 63.2; H, 6.80; N, 16.8.

Table S1. Sample and crystal data for complex **1-Tp**.

Chemical formula	$C_{31}H_{45}BCuN_7$
Formula weight	590.09
Temperature	100(2) K
Wavelength	0.71073 Å
Crystal size	0.37 x 0.33 x 0.30 mm
Crystal habit	Clear yellow prism
Crystal system	Monoclinic
Space group	P121/n1
Unit cell dimensions	a = 9.467(3) Å, α = 90°. b = 18.450(5) Å; β = 102.8°. c = 18.900(5) Å; γ = 90°.
Volume	3219.3(16) $Å^3$
Z	4
Density (calculated)	1.217 g/cm^3
Absorption coefficient	0.709 mm^{-1}
F(000)	1256

Table S2. Data collection and structure refinement for complex **1-Tp**.

Diffractometer	Bruker APEX II CCD diffractometer
Radiation source	fine-focus tube, MoKα
Theta range for data collection	1.56° to 31.50°
Index ranges	-13<=h<=13, -25<=k<=26, -27<=l<=27
Reflections collected	80400
Independent reflections	10303
Absorption correction	None
Structure solution technique	direct methods
Refinement method	Full-matrix least-squares on F2
Data / restraints / parameters	10303/0/373
Goodness-of-fit on	1.028

Table S3. Sample and crystal data for complex **2-Tp**.

Chemical formula	$C_{36}H_{49}BCuN_7$
Formula weight	654.14
Temperature	100(2) K
Wavelength	0.71073 Å
Crystal size	0.55 x 0.54 x 0.50 mm
Crystal habit	Translucent intense yellow prism
Crystal system	Monoclinic
Space group	P121/c1
Unit cell dimensions	a = 16.660(2) Å, α = 90°. b = 10.3541(14) Å; β = 93.520(2)°. c = 19.178(3) Å; γ = 90°.
Volume	3302.0(8) $Å^3$
Z	4
Density (calculated)	1.316 g/cm^3
Absorption coefficient	0.699 mm^{-1}
F(000)	1392

Table S 4. Data collection and structure refinement for complex **2-Tp**.

Diffractometer	Bruker APEX II CCD diffractometer
Radiation source	fine-focus tube, MoKα
Theta range for data collection	2.24° to 31.47°
Index ranges	-23<=h<=24, -15<=k<=14, -27<=l<=27
Reflections collected	81235
Independent reflections	10609
Absorption correction	None
Structure solution technique	direct methods
Refinement method	Full-matrix least-squares on F2
Data / restraints / parameters	10609/0/416
Goodness-of-fit on	1.078

Table S5. Sample and crystal data for complex **3-Tp**.

Chemical formula	$C_{36}H_{46}BCuN_8$
Formula weight	665.16
Temperature	100(2) K
Wavelength	0.71073 Å
Crystal size	0.40 x 0.30 x 0.20 mm
Crystal habit	Clear colorless prism
Crystal system	Triclinic
Space group	P1
Unit cell dimensions	a = 8.8871(7) Å, α = 84.0240(10)°. b = 11.1912(9) Å; β = 84.9880(10)°. c = 28.579(2) Å; γ = 71.7630(10)°.
Volume	2680.4(4) $Å^3$
Z	3
Density (calculated)	1.236 g/cm^3
Absorption coefficient	0.648 mm^{-1}
F(000)	1056

Table S6. Data collection and structure refinement for complex **3-Tp**.

Diffractometer	Bruker APEX II CCD diffractometer
Radiation source	fine-focus tube, MoKα
Theta range for data collection	1.44° to 28.28°
Index ranges	-11<=h<=11, -14<=k<=14, -37<=l<=38
Reflections collected	51831
Independent reflections	26199
Absorption correction	None
Structure solution technique	direct methods
Refinement method	Full-matrix least-squares on F2
Data / restraints / parameters	26199/1281/1301
Goodness-of-fit on	1.041

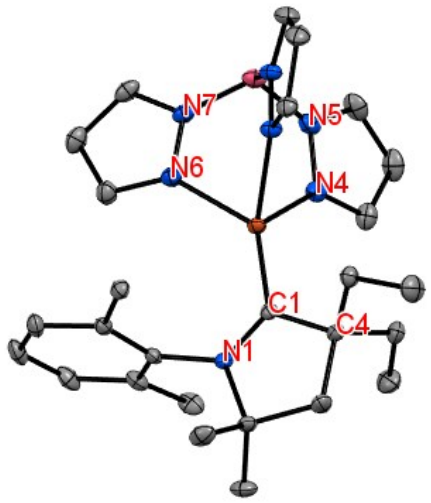

Figure S1. Oak Ridge thermal ellipsoid plot (ORTEP) representation of **1-Tp**. Thermal ellipsoids shown at 50% probability. Hydrogens and isopropyl (iPr) groups removed for clarity. The highlighted atoms are involved in relevant planes discussed in the section below.

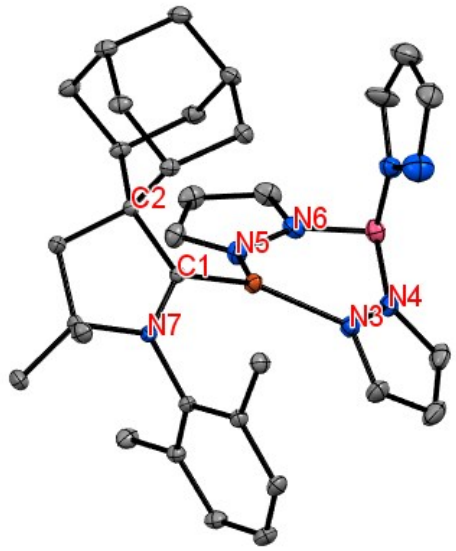

Figure S2. ORTEP representation of **2-Tp**. Thermal ellipsoids shown at 50% probability. Hydrogens and iPr groups removed for clarity. The highlighted atoms are involved in relevant planes discussed in the section below.

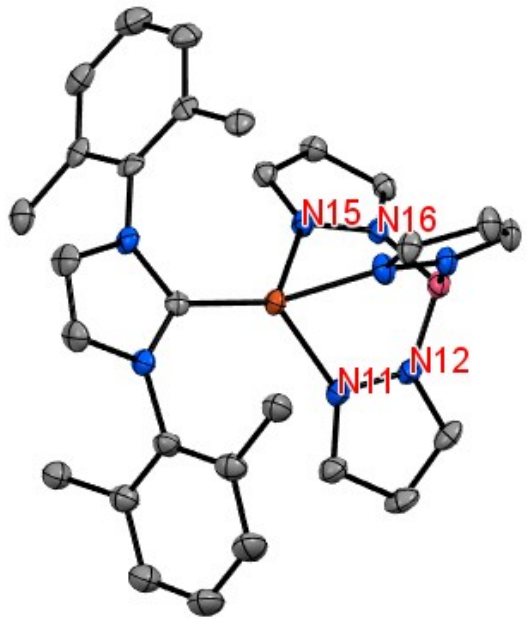

Figure S3. ORTEP representation of **3-Tp**. Thermal ellipsoids shown at 50% probability. Hydrogens and iPr groups removed for clarity. The highlighted atoms are involved in relevant planes discussed in the section below.

The Cu-N-N-B-N-N ring, formed by the Cu center and the two boron-linked pyrazole (pz) groups at a shorter distance from the metal, adopts a boat conformation in all 4 complexes. This conformation is similar to the one reported in our 3-coordinate NHC-Cu(py_2BMe_2) complexes, where the Cu-N-C-B-C-N ring is formed by the copper center and the two boron-linked pyridine groups.[10, 11] To describe the orientation of the Tp ligand with respect to the carbene, we define the following planes: For **1-Tp**: the plane encompassing C4-C1-N1 atoms of the CAAC ligand (*plane 1*) and the plane including N4-N5-N6-N7 of the pz groups at shorter bond lengths from the Cu centre. The angle formed between these two planes is referred to as angle *α*. For **2-Tp**, *α* is the angle between the following two planes: the one encompassing C2-C1-N7 of the puckered CAAC ligand (*plane 2*) and the one including N3-N4-N5-N6 of the 2 ligated pz groups. **For 3-Tp**, the two planes separated by angle *α* are the following: the NHC plane (*plane 3*) and the plane encompassing N11-N12-N15-N16 of the two pz groups at shorter bond lengths from the Cu centre. Additionally, for all three complexes, the angle formed between the aforementioned carbene planes (*planes 1, 2,* and *3*) and the plane of the pz group at the longest distance from the metal centre is referred to as angle *β*. Lastly, the angle formed between the 2,6-diisopropylphenyl (Dipp) plane and the aforementioned carbene planes (*planes 1, 2,* and *3*) in all three complexes is referred to as angle *γ*.

Table S7. Selected bond lengths and dihedral angles in complexes **1 - 3-Tp**.

	1-Tp	**2-Tp**	**3-Tp**
$C_{carbene}$-Cu	1.904(1) Å	1.886(1) Å	1.898(4) Å
Cu-N_{pz} bond lengths	2.123(1) Å; 2.138(1) Å; 2.151(1) Å	1.970(1) Å; 2.053(1) Å; 3.665(2) Å	2.093(4) Å; 2.109(3) Å; 2.145(3) Å
H_{pz}-$\pi_{(DIPP)}$ interactions	2.392 Å	2.811 Å	2.712 Å; 3.122 Å
Σ angles around Cu	337.42º	359.22º	349.47º
α	32.29º	49.12º	14.04º
β	58.48º	76.41º	87.43º
γ	89.72º	86.47º	82.02º; 82.04º

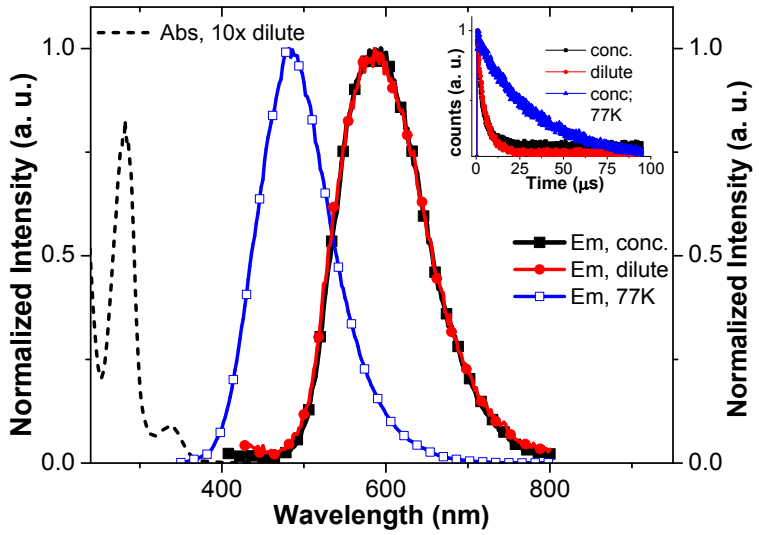

Figure S4. Figure S. Absorption (dashed line) and emission of concentrated (black, squares) and 10-fold dilute (red, circles) solutions of **1-Cl** in 2-MeTHF at room temperature and 77K (blue, open squares). The orange emission is independent of concentration as shown by the coincident spectra of the concentrated and dilute samples. The inset shows the photoluminescence (PL) decay of all three solutions, observing emission at 600 nm at RT (conc. and dilute) and 420 nm at 77K. The emission at room temperature is short-lived compared to the one at 77K, which resembles the solid-state emission. The values are reported in table S8.

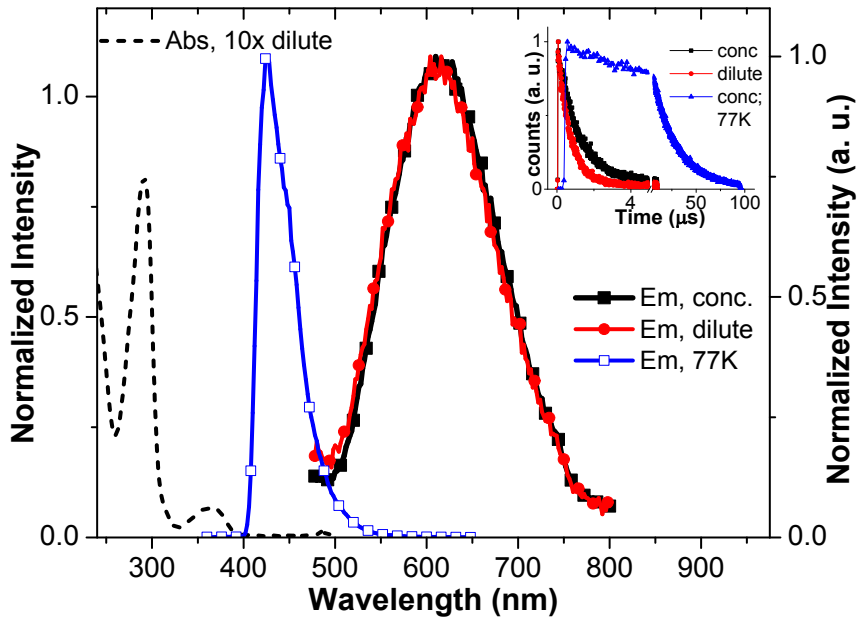

Figure S5. Absorption (dashed line) and concentration-independent emission of solutions of **2-Cl** in 2-MeTHF at room temperature (concentrated: black squares; dilute: red circles). Emission of the concentrated solution at 77K (blue, open squares) resembles the solid-state emission, and has a similar PL decay as shown in the inset (blue triangles; recorded at 420 nm). The room temperature emission for the concentrated and dilute solutions (black squares and red circles respectively, recorded at 600 nm) is short-lived compared to that at 77K. The values are reported in table S8.

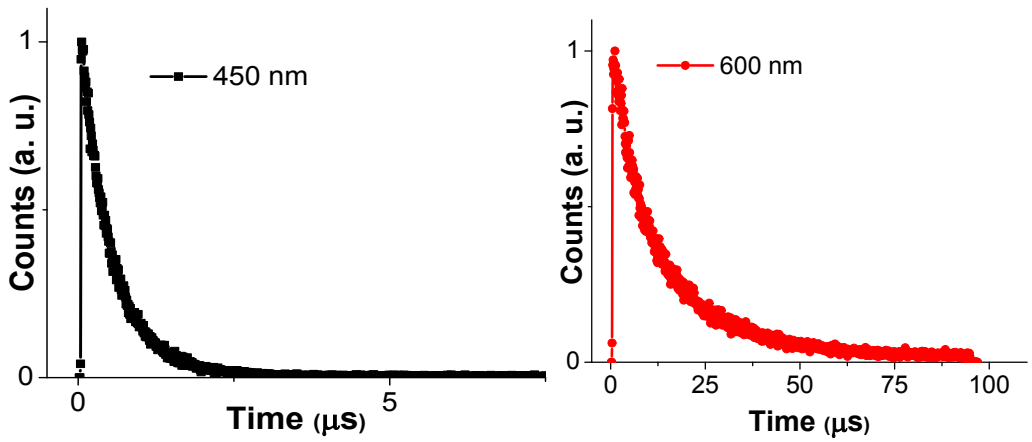

Figure S6. PL decay of a concentrated solution of **1-Cl** in MeCy.

The lifetime of the high-energy feature is shown on the left (black squares) and is shorter-lived than the that of the low-energy component shown on the right (red circles).

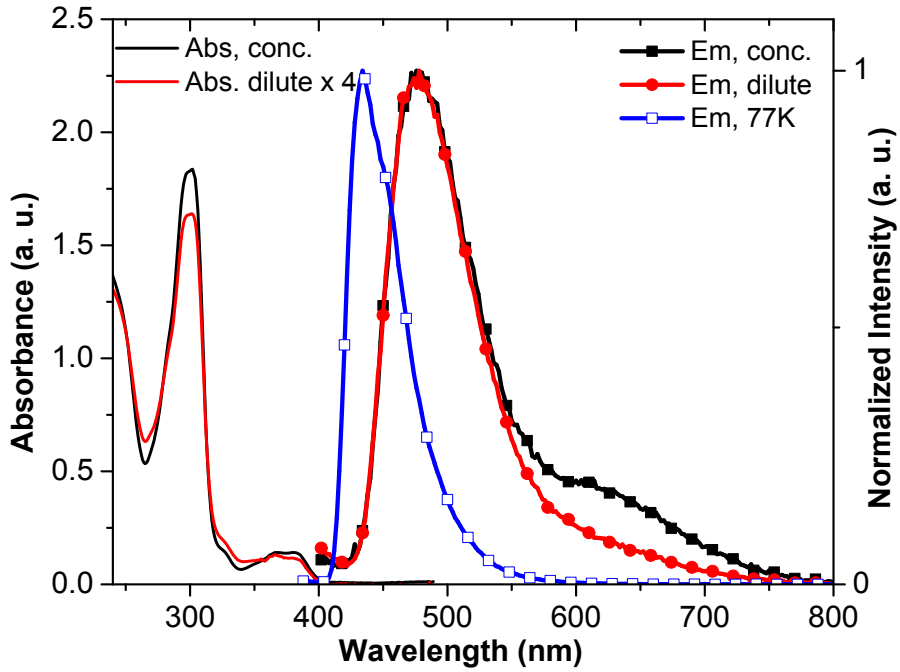

Figure S7. Absorption (solid lines) and emission (symbols) of concentrated (black, squares) and dilute (red, circles) solutions of **2-Cl** in MeCy at room temperature (red and black) and 77K (blue, open squares).

In addition to the high-energy component, the concentrated solution emission shows a lower-energy component that becomes less pronounced upon dilution. This is consistent with excimer formation, and the interaction does not occur in the frozen solution.

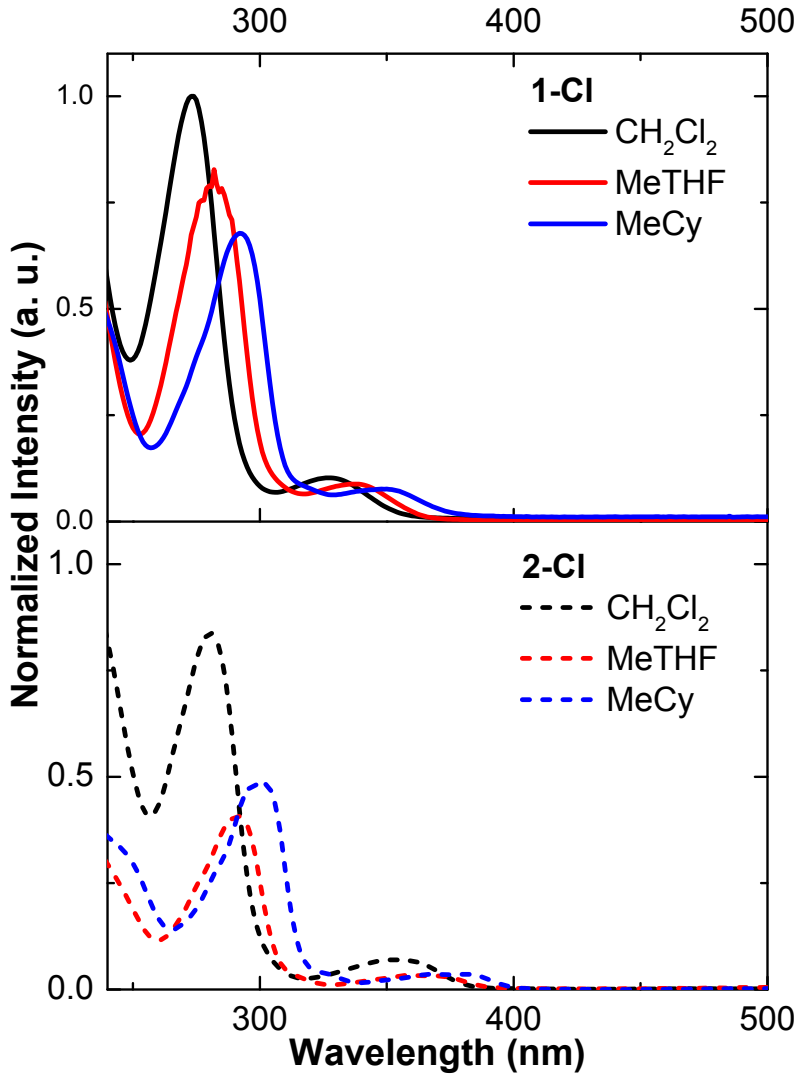

Figure S8. Normalized absorption spectra of **1-Cl** (solid lines, top) and **2-Cl** (dashed lines, bottom) in CH_2Cl_2 (black), 2-MeTHF (red), and MeCy (blue).

The trace for **1-Cl** in MeCy is multiplied by 3 for clarity. The two complexes show negative solvatochromism, characterized by a blue shift in more polar solvents.

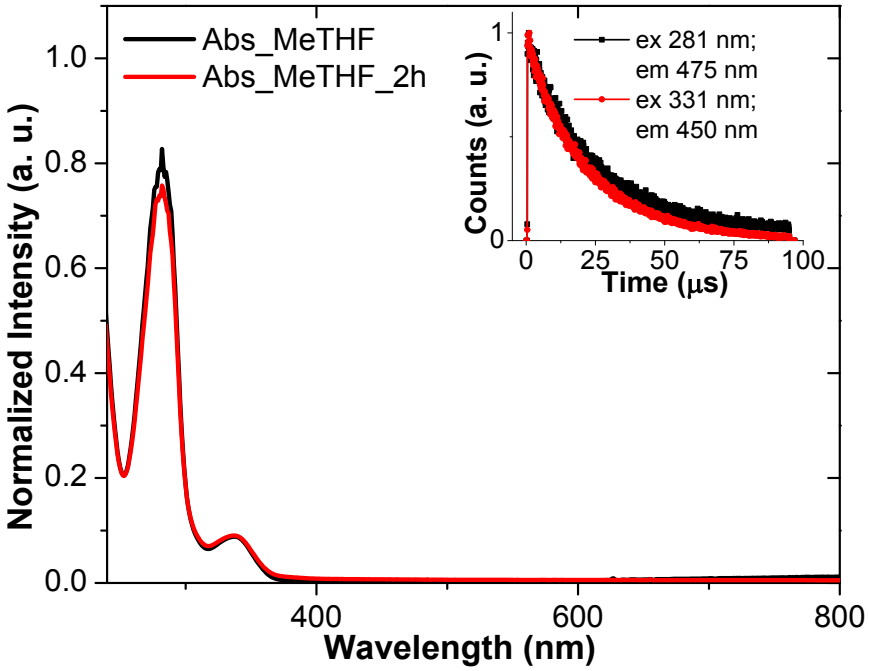

Figure S9. Absorption spectra of **1-Cl** in 2-MeTHF before (black) and after (red) 2h of irradiation at 305 nm, 281 nm, and 331 nm.

The inset shows the PL decay of the microcrystalline sample after 40 minutes of irradiation at 281 nm followed by 40 minutes of irradiation at 331 nm. Both measurements show no signs of photodecomposition.

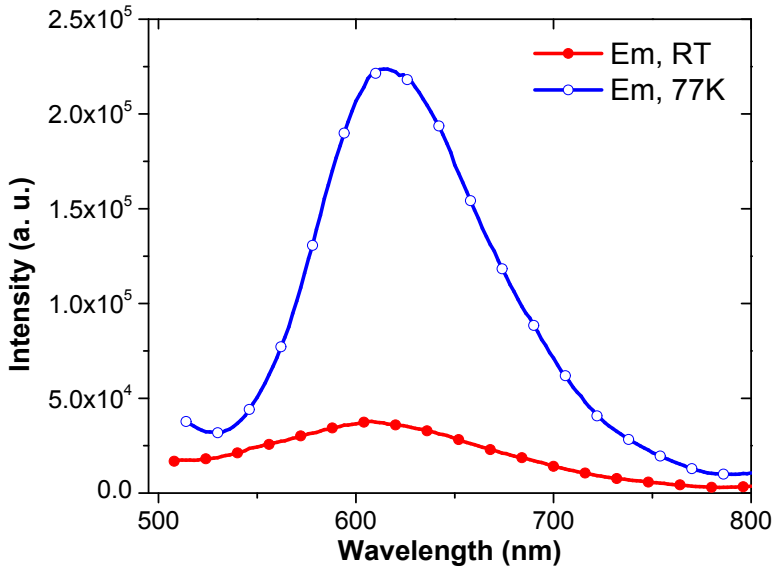

Figure S11. Emission spectra of a crystalline sample of **2-Tp** at RT and 77K.

Slit widths, excitation wavelength (360 nm), and sample position were kept constant in the two measurements. Taking into account the refractive index of the LN_2 medium in the dewar at 77K (1.20),[1] the room temperature measurement was done with acetone in the dewar. The refractive index of acetone at room temperature (1.36)[2] is comparable to that of LN_2.

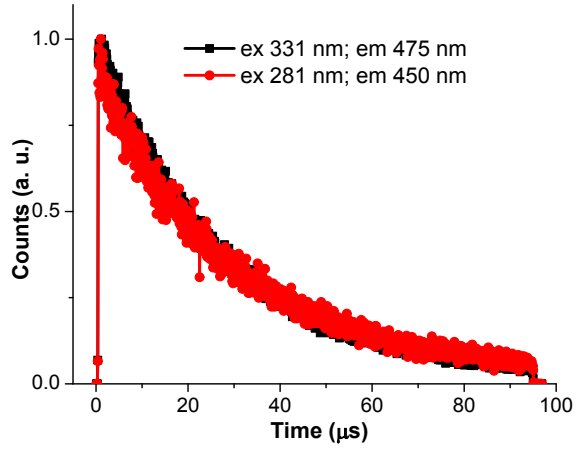

Figure S10. PL decays of a microcrystalline sample of **2-Cl**; one with 40 minutes of irradiation at 331 nm (black) followed by 40 minutes of irradiation at 281 nm (red).

The identical traces show no signs of photodecomposition of the sample.

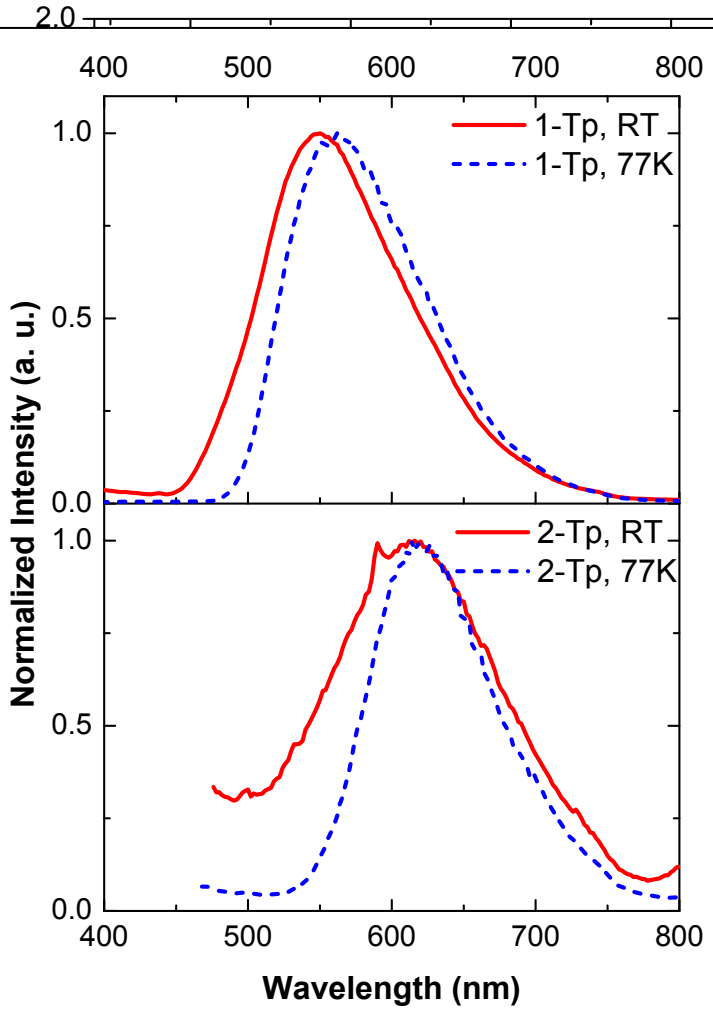

Figure S13. Emission spectra of crystals of **1-Tp** and **2-Tp** at RT (red, solid) and 77K (blue, dashed). Little spectral shift is observed upon cooling.

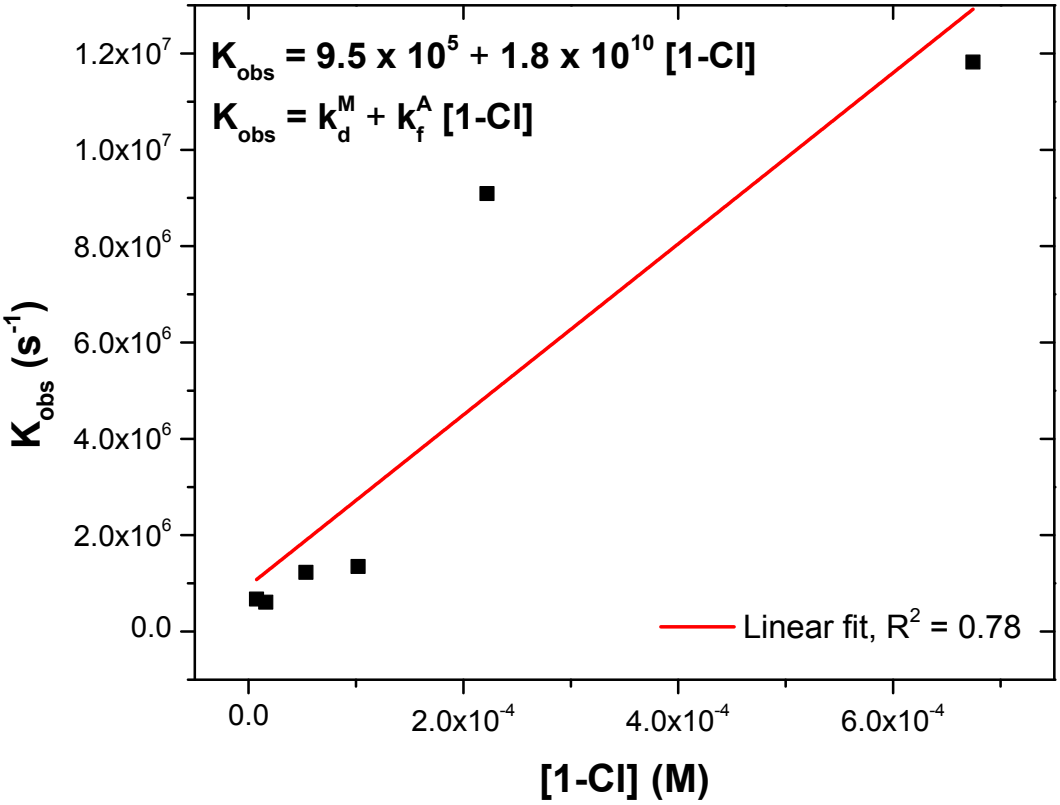

Figure S14. Modified Stern-Volmer plot of self-quenching kinetics for **1-Cl** in MeCy. Due to poor solubility limits, the concentrations were determined using the extinction coefficients of the high-energy absorption peak of the complex in CH_2Cl_2. The equation displayed in the figure corresponds to a kinetic model where the monomeric species (M) forms an aggregate species (A), with a rate constant of formation, k_f^A = 1.8 x 10^{10} s^{-1}. The emission decay rate of the monomer at infinite dilution has a rate constant of k_d^M = 9.5 x 10^5 s^{-1}, as given by the intercept of the linear fit. Excitation spectra corresponding to emission at 650 nm of the more concentrated samples show a clear peak at 528 nm. The PL decays at 650 nm for all the concentrations examined show no discernable rise time. These observations, together with k_f^A = 1.8^{10} s^{-1}, indicate the formation of an aggregate species of

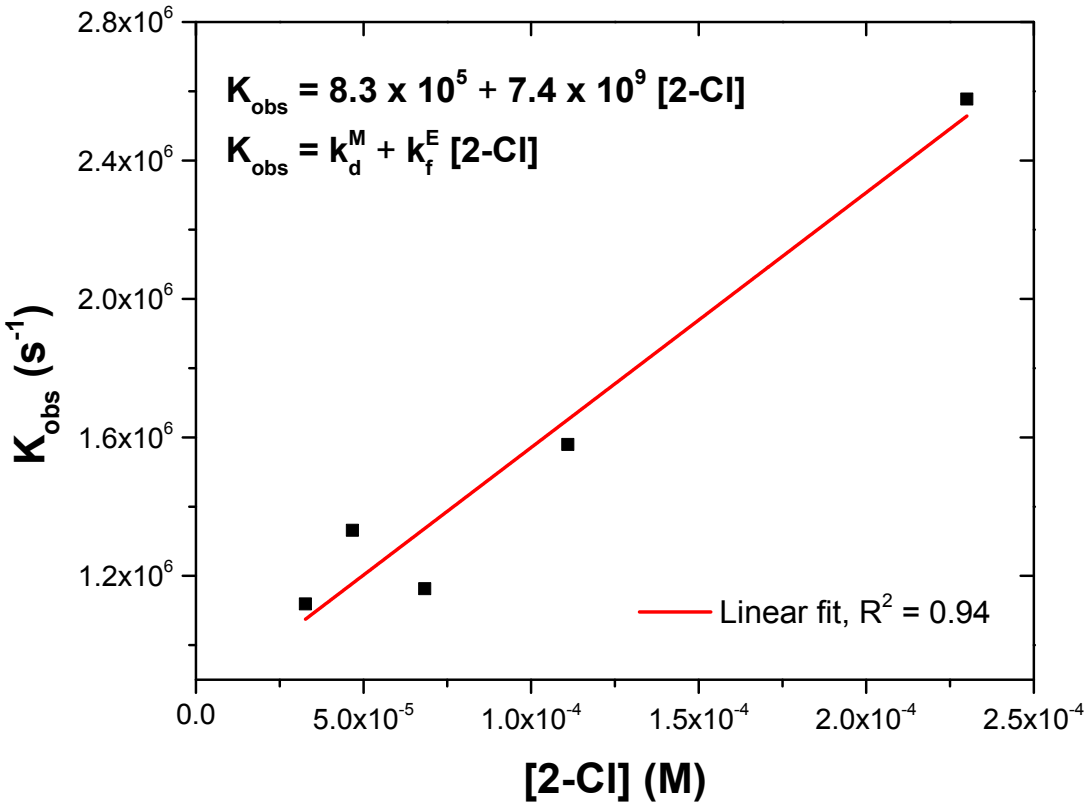

Figure S15. Modified Stern-Volmer plot of self-quenching kinetics for **2-Cl** in MeCy. Due to poor solubility limits, the concentrations were determined using the extinction coefficients of the high-energy absorption peak of the complex in CH_2Cl_2. The equation displayed in the figure corresponds to a kinetic model where the monomeric species (M) forms an excimer (E), with a rate constant of formation, k_f^E = 7.4 x 10^9 s^{-1}. The emission decay rate of the monomer at infinite dilution has a rate constant of k_d^M = 8.3 x 10^5 s^{-1}, as given by the intercept of the linear fit. Excitation spectra corresponding to emission at 650 nm are identical to those corresponding to emission at 430 nm. The PL decay at 650 nm shows a rise time that is concentration-dependent. These observations, together with k_f^E = 7.4 x 10^9 s^{-1}, indicate a diffusion-limited excimer formation process for **2-Cl** in MeCy.

Table S8. Photophysical properties of **1-Cl** and **2-Cl** in concentrated and dilute solutions of MeCy and 2-MeTHF.

The reported results show concentration-dependent emission in the former solvent and not in the latter. Excited state interactions in the solutions at room temperature no longer occur upon cooling to 77K.

	RT				**77K**		
Complex	**Solution**	**τ (μs) (nm)***	**Φ_{PL}**	**λ_{max}** (nm)**	**Solution**	**τ (μs) (nm)***	**λ_{max} (nm)**
1-Cl	MeCy; conc.	• 0.52 (451 nm) • 5.0 (20%); 18 (80%) (600 nm)	0.19	442; 570	MeCy; conc.	32 (475 nm)	456
	MeCy; 5x dilution	• 0.41 (451 nm) • 8.1 (57%); 22.8 (43%) (600 nm)	0.17		MeCy; 5x dilution	30 (475 nm)	
	2-MeTHF; conc.	4.2 (600 nm)	0.08	594	2-MeTHF; conc.	33 (550 nm)	482
	2-MeTHF; 10x dilution	4.6 (600 nm)	0.08		2-MeTHF; 10x dilution	33 (550 nm)	
2-Cl	MeCy, conc.	• 0.54 (475 nm) • 0.42 (-29%); 1.34 (129%) (650 nm)	0.03	476; 614	MeCy; conc.	32 (500 nm)	434
	MeCy; 4x dilution	• 1.23 (475 nm) • 0.93 (-124%); 1.33 (224%) (650 nm)	0.04		MeCy; 4x dilution	28 (450 nm)	
	2-MeTHF; conc.	0.58 (600 nm)	0.015	610	2-MeTHF; conc.	28 (475 nm)	426
	2-MeTHF; 10x dilution	0.69 (600 nm)	0.016		2-MeTHF; 10x dilution	28 (475 nm)	

*The lifetimes (μs) are reported with the wavelengths (nm) at which they were recorded. **In MeCy at RT, λ_{max} values are reported for both, the high-energy peak as well as the low-energy one observed.

Table S9. Lowest energy transitions for complexes **1 - 3-Tp** obtained from TDDFT calculations. While fully optimized structures were used for **1-** and **3-Tp**, for **2-Tp** the geometry was optimized while keeping the dihedral angle formed between the carbene and Tp ligands frozen at 43.0°.

Also shown is the calculated ΔE_{S1-T1}, too large for thermally activated delayed fluorescence to occur. This result is in agreement with the photophysical properties shown in Fig. S13.

Complex	**State**	**Vertical excitation**	**Oscillator strength**	**Major contribution***	**ΔE_{S1-T1}**
1-Tp	S_1	3.34 eV	0.0037	HOMO→LUMO (88%) HOMO-1→LUMO (10%)	470 meV
	T_1	2.87 eV	0.0000	HOMO→LUMO (92%)	
2-Tp	S_1	3.19 eV	0.0096	HOMO→LUMO (76%) HOMO-3→LUMO (19%)	510 meV
	T_1	2.68 eV	0.0000	HOMO→LUMO (90%)	
3-Tp	S_1	3.80 eV	0.0037	HOMO→LUMO+1 (59%) HOMO→LUMO+4 (36%)	270 meV
	T_1	3.53 eV	0.0000	HOMO→LUMO+4 (41%) HOMO→LUMO+1 (35%) HOMO-1→LUMO+4 (13%)	

*transitions with ≥10% contribution

Table S10. Frontier orbitals and triplet spin densities of complexes **1 - 3-Tp**.

Complex	**HOMO (red) and LUMO (blue)**	**Select frontier orbitals contributing to transitions**		**Spin density**	**Optimized S_0 (black) and T_1 (red)**
1-Tp	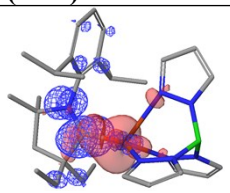 E_{HOMO} = -5.38 eV E_{LUMO} = -0.74 eV	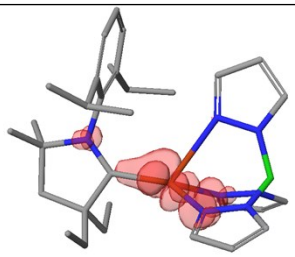 E_{HOMO-1} = -5.41 eV		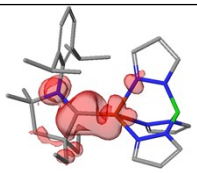 iso value = 0.00258	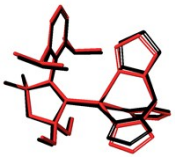
2-Tp	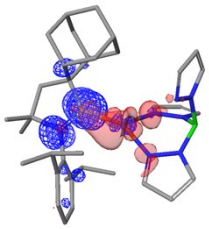 E_{HOMO} = -5.48 eV E_{LUMO} = -1.10 eV	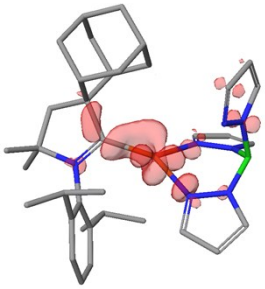 E_{HOMO-3} = -5.79 eV		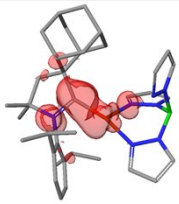 iso value = 0.00265	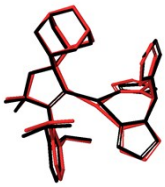
3-Tp	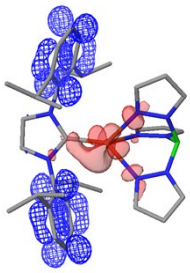 E_{HOMO} = -5.08 eV E_{LUMO} = -0.40 eV	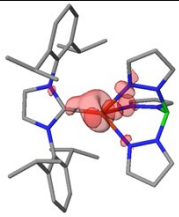 E_{HOMO-1}= -5.24 eV	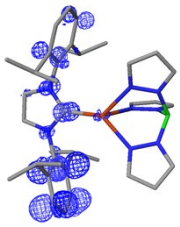 E_{LUMO+1} = -0.31 eV 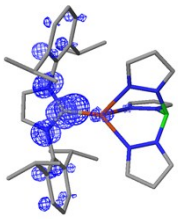 E_{LUMO+4} = 0.16 eV	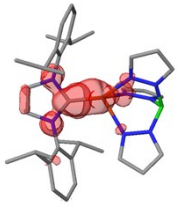 iso value = 0.0030	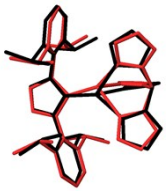

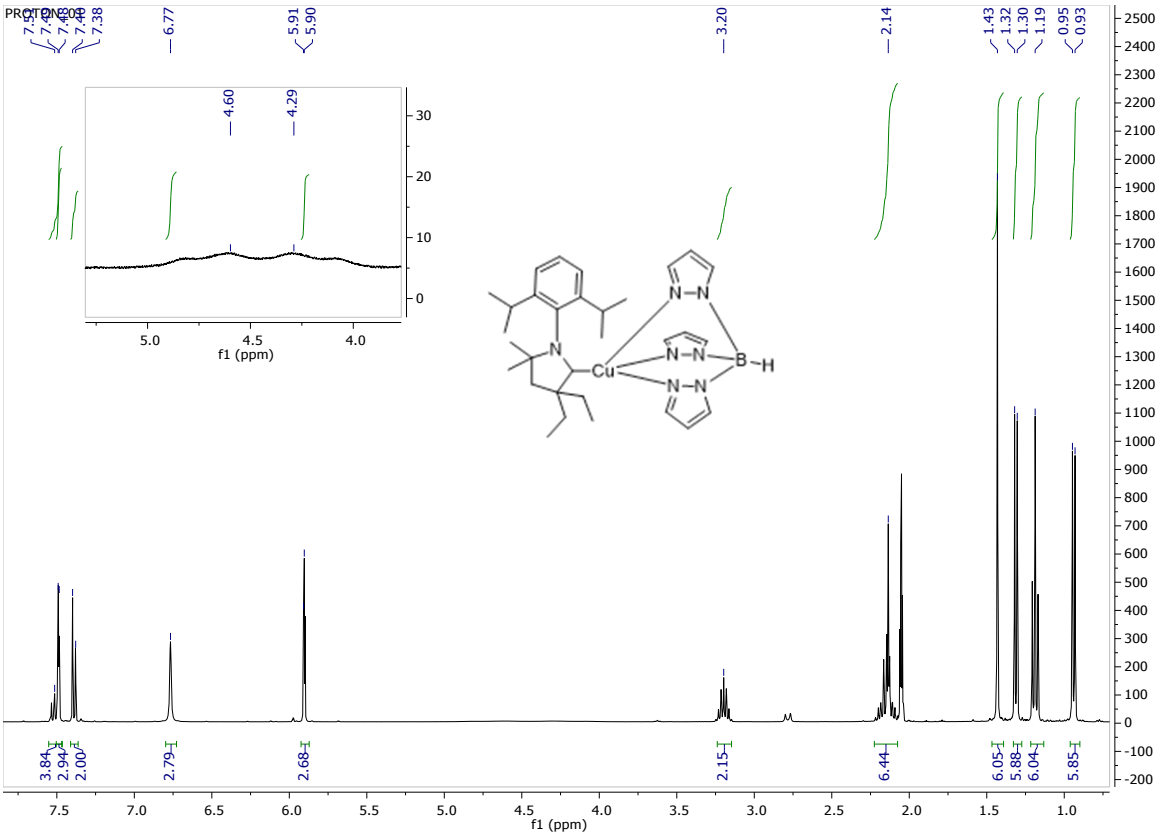

Figure S16. ^{1}H NMR of **1-Tp** in acetone d_6.

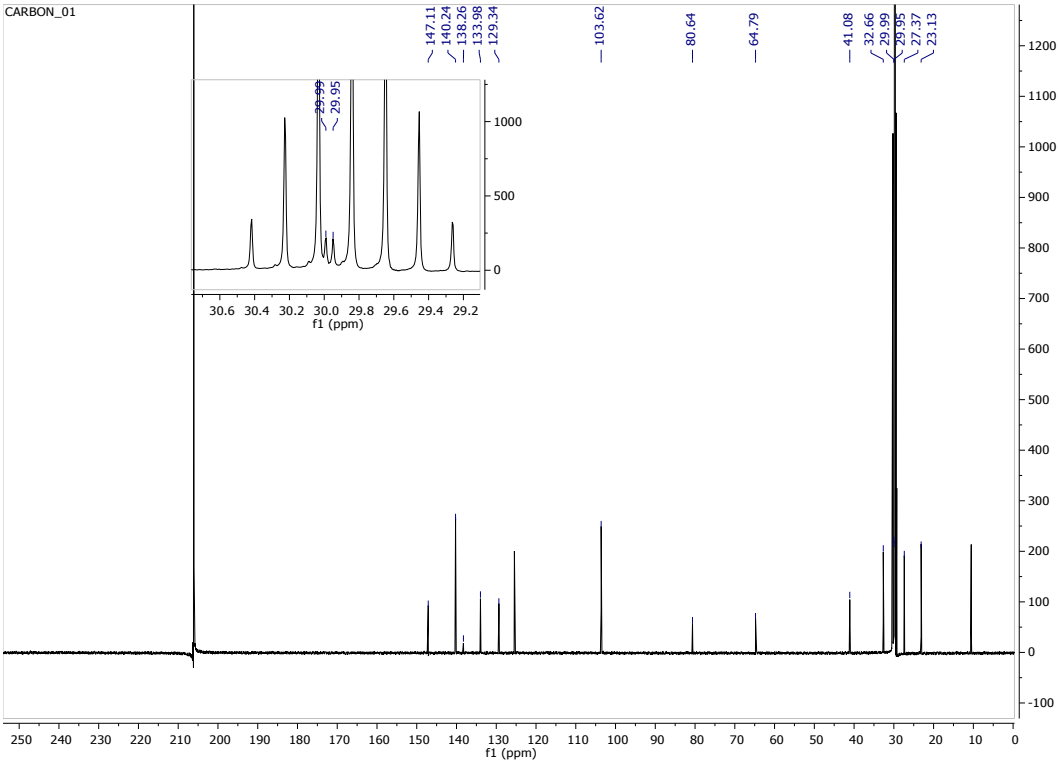

Figure S17. ^{13}C NMR of **1-Tp** in acetone d_6.

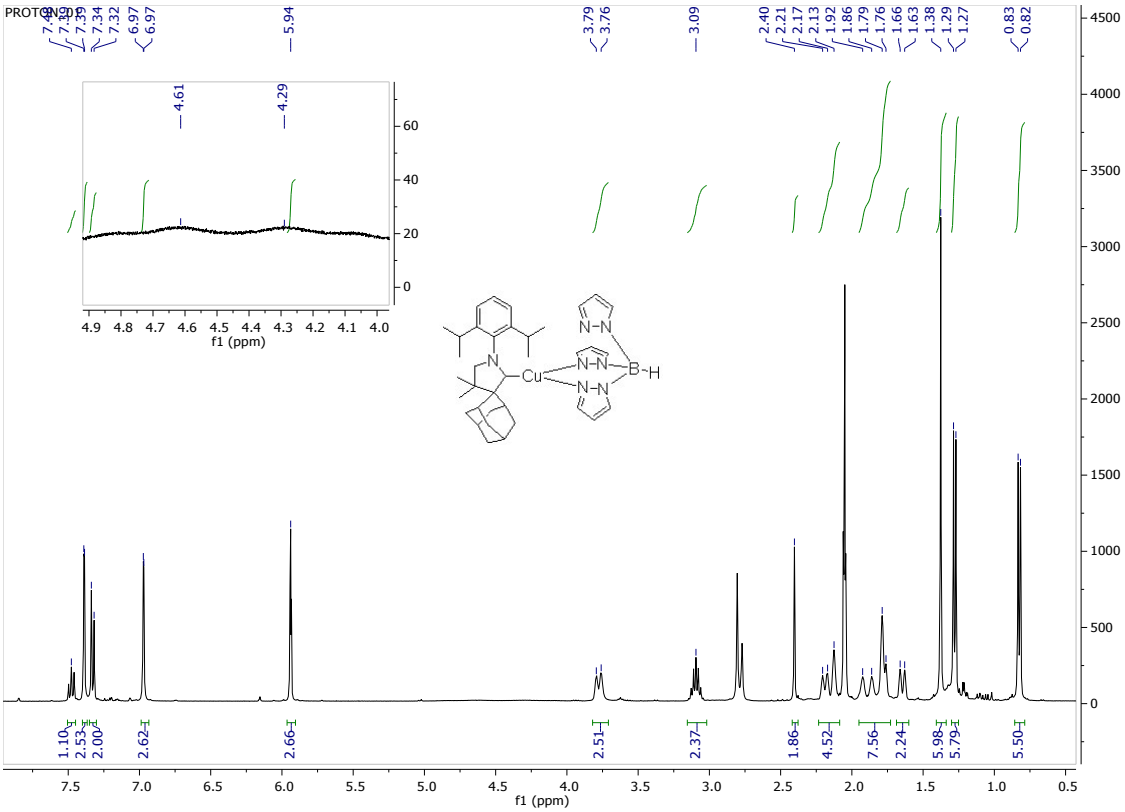

Figure S 18. ^{1}H NMR of **2-Tp** in acetone d_6.

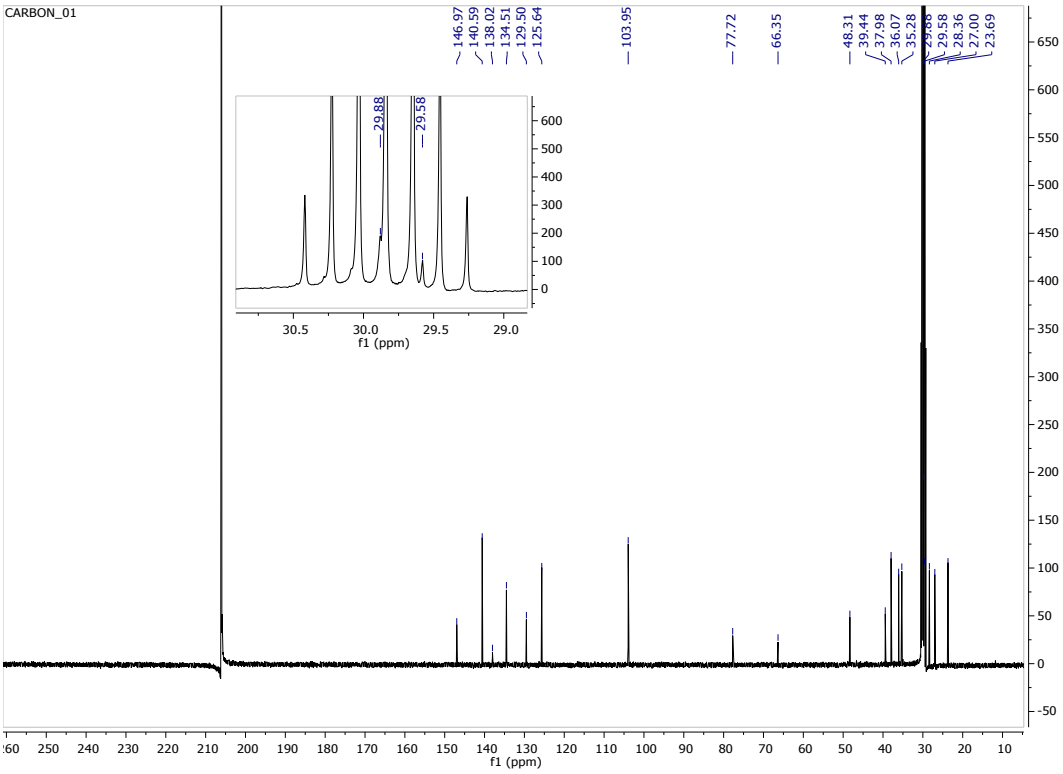

Figure S19. ^{13}C NMR of **2-Tp** in acetone d_6.

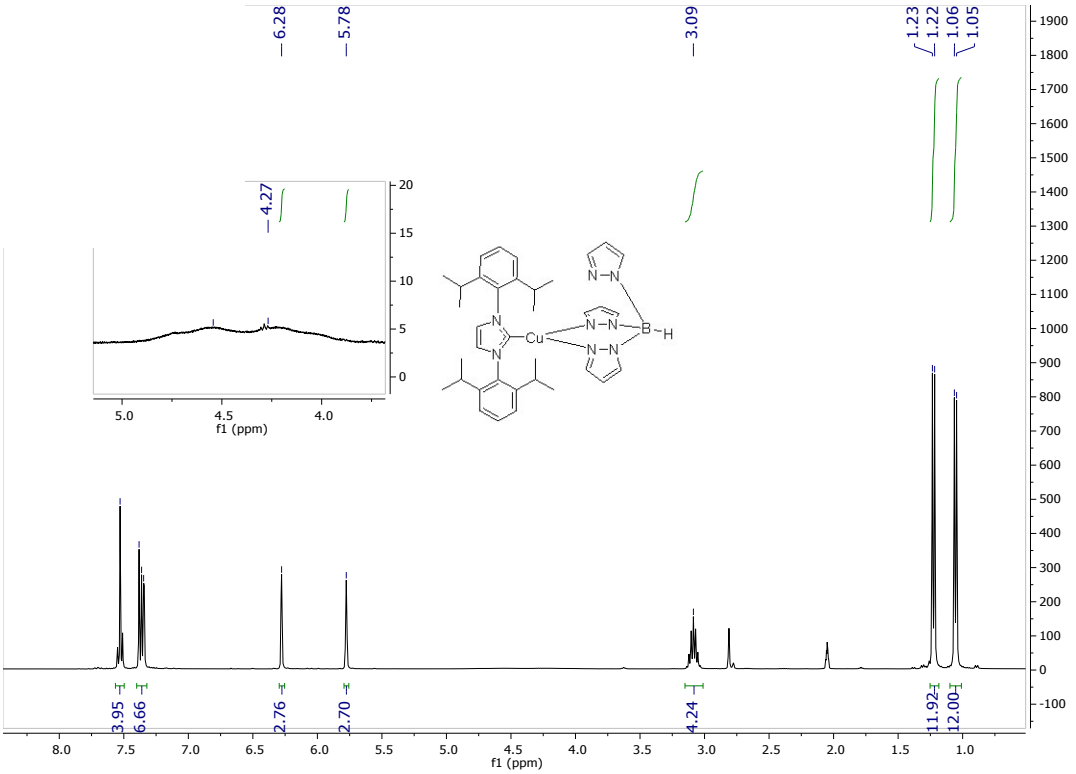

Figure S20. ^{1}H NMR of **3-Tp** in acetone d_6.

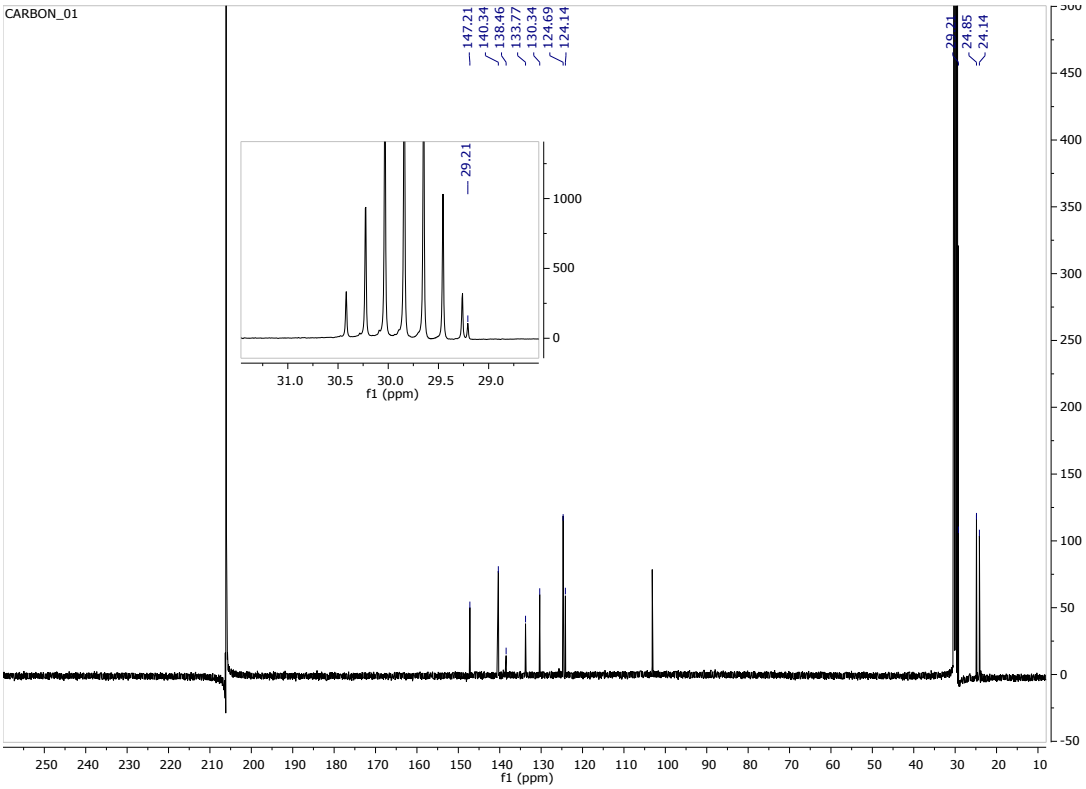

Figure S21. ^{13}C NMR of **3-Tp** in acetone d_6.

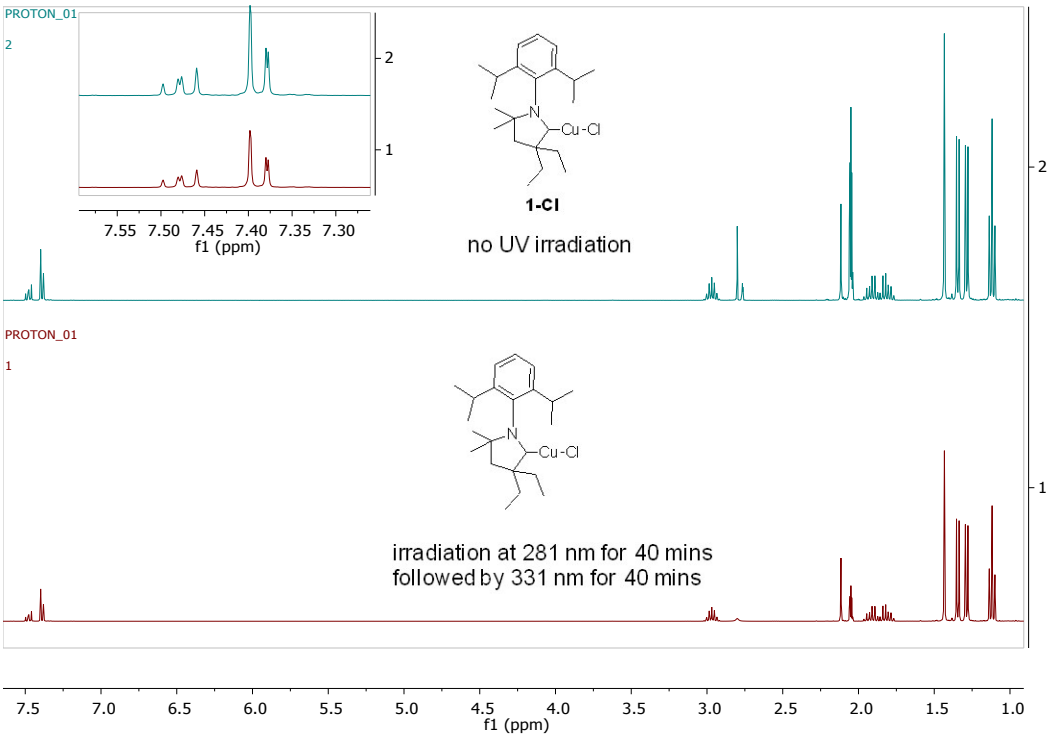

Figure S22. ^{1}H NMR of **1-Cl** in acetone d_6 with and without UV- irradiation.

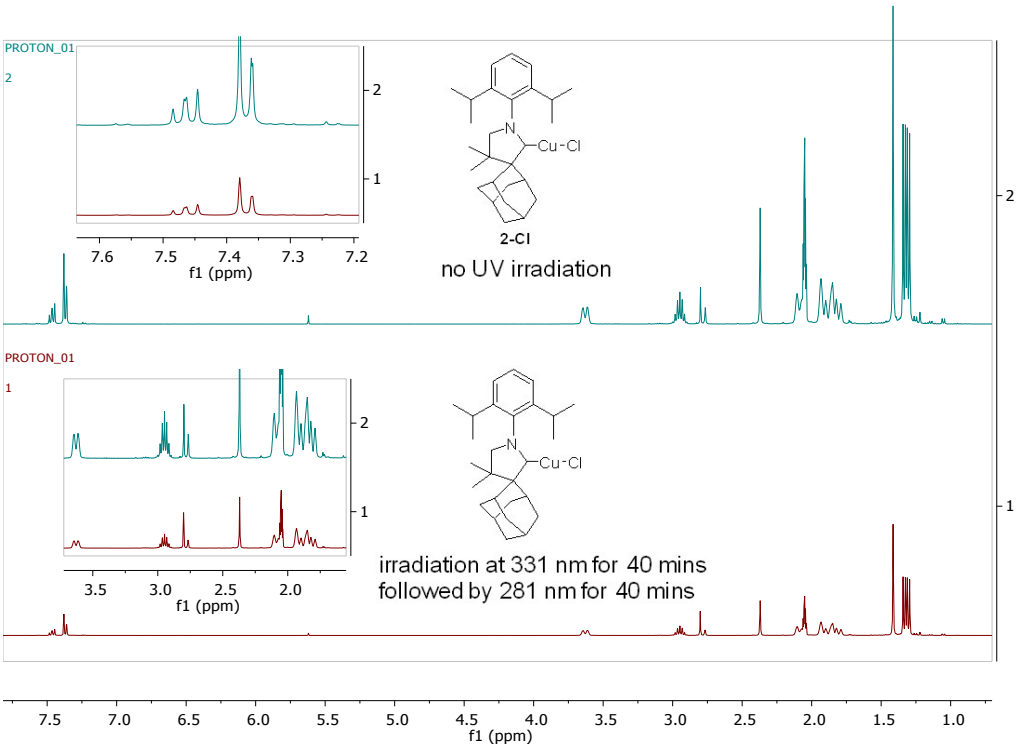

Figure S23. ^{1}H NMR of **2-Cl** in acetone d_6 with and without UV irradiation.

References.

1. H. E. Johns and J. O. Wilhelm, *Canadian Journal of Research*, 1937, **15a**, 101-108.
2. S. S. Kurtz Jr., A. E. Wikingsson, D. L. Camin and A. R. Thompson, *Journal of Chemical and Engineering Data*, 1965, **10**, 330-334.
3. A. S. Romanov, D. Di, L. Yang, J. Fernandez-Cestau, C. R. Becker, C. E. James, B. Zhu, M. Linnolahti, D. Credgington and M. Bochmann, *Chemical Communications*, 2016, **52**, 6379-6382.
4. G. D. Frey, R. D. Dewhurst, S. Kousar, B. Donnadieu and G. Bertrand, *Journal of Organometallic Chemistry*, 2008, **693**, 1674-1682.
5. X. B. Hu, M. Soleilhavoup, M. Melaimi, J. X. Chu and G. Bertrand, *Angewandte Chemie-International Edition*, 2015, **54**, 6008-6011.
6. A. D. Bochevarov, E. Harder, T. F. Hughes, J. R. Greenwood, D. A. Braden, D. M. Philipp, D. Rinaldo, M. D. Halls, J. Zhang and R. A. Friesner, *International Journal of Quantum Chemistry*, 2013, **113**, 2110-2142.
7. A. D. Becke, *Journal of Chemical Physics*, 1993, **98**, 5648-5652.
8. C. T. Lee, W. T. Yang and R. G. Parr, *Physical Review B*, 1988, **37**, 785-789.
9. P. J. Hay and W. R. Wadt, *Journal of Chemical Physics*, 1985, **82**, 299-310.
10. V. A. Krylova, P. I. Djurovich, J. W. Aronson, R. Haiges, M. T. Whited and M. E. Thompson, *Organometallics*, 2012, **31**, 7983-7993.
11. V. A. Krylova, P. I. Djurovich, B. L. Conley, R. Haiges, M. T. Whited, T. J. Williams and M. E. Thompson, *Chemical Communications*, 2014, **50**, 7176-7179.